ORIGINAL ARTICLE

A least-squares identification method for vehicle cornering stiffness identification from common vehicle sensor data.

T. Devos[a,b] and F. Naets[a, b]

[a]E2E Lab, Flanders Make@KU Leuven; [b]Department of Mechanical Engineering, KU Leuven, Belgium

ARTICLE HISTORY
Compiled July 7, 2023

ABSTRACT
In this study, we present a robust framework for vehicle tire cornering stiffness identification, leveraging commonly available lateral acceleration and yaw rate measurements. In contrast to most of the state-of-the-art approaches, our methodology does not rely on (augmented) state estimation, but on batch least-squares optimization of larger time windows. This batch-approach has as a major benefit that many of the observability issues which are encountered in estimation-based methods are completely eliminated. By immediately exploiting the measurement equations, rather than comparing dynamic simulation responses, we obtain a very efficient and sparse formulation which enables online processing. The methodology was validated on (openly available) datasets from two different vehicles – a Ferrari 250LM and Range Rover Evoque, delivering consistent and accurate results for both vehicles. This work shows that batch optimization can be a very promising alternative for the more common state-estimation approaches for extracting reliable vehicle cornering stiffnesses in various driving scenarios with a much more straightforward tuning.

KEYWORDS
Cornering stiffness identification, least-squares optimization, vehicle dynamics

1. Introduction

In the past few decades, both driver assistance and (semi-)active safety systems have become widely adopted standards within the automotive industry [2]. The precision of system parameters is vital for optimal vehicle performance, particularly tire parameters which significantly influence vehicle dynamics. However, accurately measuring these parameters proves to be both challenging and costly due to their high dependence on current vehicle and environmental conditions. Despite the existence of numerous models, linear models have been proven to offer a solid representation for the majority of standard applications, including spirited driving. Direct measurement of these variables demands expensive equipment such as optical speed sensors and force measuring wheels [1], rendering them impractical for commercial vehicles.

At present, tire handling parameters are primarily obtained through comprehensive offline testing [20,25], which facilitates detailed model comparisons utilized in vehicle design. However, these predetermined parameters are of limited use during a vehicle's life cycle as changing road conditions and tire wear significantly affect performance.

CONTACT F. Naets. Email: frank.naets@kuleuven.be

Accurate, real-time knowledge of tire properties can greatly enhance vehicle performance optimization.

Existing cornering stiffness estimation methodologies for operational conditions mainly employ estimator-based approaches such as Kalman filtering, which concurrently estimate sideslip angles and forces using known models [6,16,28]. Ray proposed an approach that combines sideslip angle and tire parameter estimation via an extended Kalman filter [21,22]. Here, a joint estimator is utilized to directly estimate the different tire forces in conjunction with the model states. Subsequent researchers have developed variations on these estimation schemes aiming to concurrently estimate sideslip and tire parameters [5]. Some have suggested alternative sensor-based methods such as a 2-antenna GPS sensor for sideslip angle estimation [23] or steering torque sensors in electric power-assisted steering systems [29]. The primary advantage of these estimation methodologies is their potential for real-time or near real-time vehicle applications. However, a common challenge is the effective tuning of the estimator which can differ considerably across vehicles, and ensuring robust operation during low-excitation maneuvers. Dedicated schemes have been proposed to ensure this robust operation, but they may demand additional tuning requirements (e.g. [17]).

Data-driven approaches to characterizing vehicle dynamics behavior are also worth noting. Several authors have proposed general system identification approaches to model vehicle cornering behavior [4,27]. Although these methods successfully predict vehicle behavior, they lack the physical interpretability of their first-principles model-based counterparts.

Alternatively, a more traditional identification scheme can be applied where a batch of measurement data is compared to the predictions of a parameterized vehicle model. The parameters are adjusted until the best fit, typically in a least squares sense, is obtained. This approach eliminates the tuning required in estimation-based methods. While several authors have discussed this scheme (e.g. [27]), it does not appear to be common in the literature. This may be attributed to two primary reasons: the relatively high computational effort due to the need to integrate the equations of motion and compute their derivatives, and the potential difficulty in convergence due to the non-convexity of the resulting problem.

In this paper, we present an approach based on batch-identification methods for vehicle dynamics. The method assumes linear tire behavior, which is prevalent in the majority of common driving scenarios, and an equivalent bicycle model behavior for the vehicle. Instead of using a simulation to perform the identification, we propose directly executing a concurrent identification of both the front and rear cornering stiffnesses and the lateral velocities of the vehicle at various timesteps of interest. For each considered timestep, our objective is to minimize the error with respect to two commonly available vehicle measurements, namely the lateral acceleration and the yaw rate. Although this represents a large-scale problem for long time series, the straightforward nature of the equations allows for highly efficient computation. This leads to a scheme that evaluates an order of magnitude faster than the considered time series. A key aspect that we investigate is the influence of the relative importance of the weight assigned to the two types of measurements in a weighted least-squares sense.

The method is shown to perform well on two experimental datasets, and when a forward simulation is executed using the identified parameters, the vehicle response is practically coincident with the measured behavior.

In the first section, we discuss the conceptual bicycle model and the different steps in the batch-solution-based identification problem. Subsequently, the validation is per-

formed using two freely available vehicle dynamics datasets, resulting in a very reliable estimation with minimal tuning.

2. Batch-solution based cornering-stiffness optimization problem

This section investigates the developed cornering stiffness identification scheme. We initially describe the bicycle model that is utilized for deriving the identification framework and linking the parameters to various measurements. Subsequently, we explicate how the lateral acceleration and yaw rate measurements can be leveraged to concurrently extract the front and rear cornering stiffnesses and lateral velocities. Lastly, we briefly discuss a least-squares approach as a solution to the identification problem.

2.1. Bicycle vehicle model overview

The identification scheme we propose is based on a dynamic vehicle model. Given the limitations on available measurements and a primary interest in fundamental cornering dynamics, we have opted for the bicycle model. This model, originally proposed by Segel in 1956 [24], serves as the foundation of our approach (see Fig. 1).

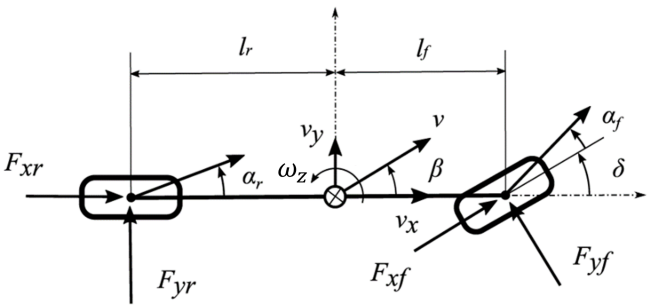

Figure 1. The bicycle vehicle dynamics model.

The various states and variables incorporated into this model are as follows:

- ω_z represents the yaw rate around the center-of-gravity (COG),
- v_x and v_y denote the longitudinal and lateral velocities of the COG of the vehicle, projected onto a vehicle-fixed frame, with v signifying the resultant velocity vector,
- β signifies the sideslip angle at the COG,
- α_f and α_r are the front and rear wheel sideslip angles, respectively,
- F_{xf}, F_{yf} denote the longitudinal and lateral forces exerted on the front tire, whereas F_{xr}, F_{yr} represent the longitudinal and lateral forces acting on the rear tire (all described in a tire-attached frame),
- δ stands for the steering angle,
- l_f and l_r denote the distances from the COG to the front and rear axle, respectively.

The selection of the bicycle model is a crucial one. It presupposes that the average tire forces acting on the front and rear axles predominantly influence the vehicle's behavior. This is a calculated trade-off. Employing a conventional four-wheel model

would not enable the segregation of the left and right forces without previous assumptions regarding their distribution. Additionally, we assume a small steering angle. This assumption decouples the longitudinal and lateral dynamics of the bicycle model, permitting us to focus solely on the lateral vehicle dynamics within the identification scheme. In this scenario, the lateral vehicle dynamics, using the lateral velocity and yaw rate as states, can be articulated as follows:

$$\dot{v}_y = \frac{1}{m}\left(F_{yf} + F_{yr}\right) - v_x\omega_z, \tag{1a}$$

$$\dot{\omega}_z = \frac{1}{I_z}\left(l_f F_{yf} - l_r F_{yr}\right), \tag{1b}$$

where m denotes the vehicle mass and I_{zz} represents the yaw moment of inertia. Both these variables are assumed known. It's important to note that since this model considers the attached lateral vehicle velocity as the primary state, Eq. (1a) also includes a gyroscopic contribution from the yaw-rate and longitudinal velocity. In Eq. (1), we treat the longitudinal velocity v_x as an input, which, for example, can be approximately extracted from wheel speed measurements. A secondary key assumption in this work is the linear behavior of the lateral tire forces F_y:

$$F_{yf} = -c_{yf}\alpha_f = -c_f\left(\frac{v_{yf}}{v_x} - \delta\right), \tag{2a}$$

$$F_{yr} = -c_{yr}\alpha_r = -c_r\frac{v_{yr}}{v_x}, \tag{2b}$$

with front and rear cornering stiffness c_f, c_r and wheel sideslip angle α. The front- and rear-sideslip velocities are evaluated as:

$$v_{yf} = v_y + l_f\omega_z,\ v_{yr} = v_y - l_r\omega_z. \tag{3}$$

The resulting dynamic system equations can be summarized as:

$$\begin{bmatrix}\dot{v}_y\\ \dot{\omega}_z\end{bmatrix} = \begin{bmatrix}\frac{1}{mv_x}(-c_f - c_r) & \frac{1}{mv_x}(-l_f c_f + l_r c_r) - v_x\\ \frac{1}{I_z v_x}(-l_f c_f + l_r c_r) & \frac{1}{I_z v_x}(-l_f^2 c_f + l_r^2 c_r)\end{bmatrix}\begin{bmatrix}v_y\\ \omega_z\end{bmatrix} + \begin{bmatrix}\frac{1}{m}c_f\\ \frac{1}{I_z}l_f c_f\end{bmatrix}\delta. \tag{4}$$

Starting from this system of equations, we will examine in the next section which quantities are known and unknown when we try to identify the linear cornering stiffnesses for this system.

2.2. Measurement goal functions for lateral dynamics identification

In order to devise a suitable identification framework, we must determine which states and parameters in this dynamic model are known and which are unknown. Moreover, it is essential to assess which measurements might be available to guide the fitting function for this problem, such that we obtain an identifiable problem [8].

Regarding parameters, we presume the mass m, yaw inertia I_z, and the position of the COG (l_f and l_r) for the vehicle to be known. In practice, these quantities can exhibit variations due to differing payloads and payload locations within the vehicle. Fortunately, in regular automotive applications, this ratio can be assumed to be mi-

nor, and an average value for these quantities should provide a sufficiently accurate approximation.

Next, we consider the available input measurements for the identification problem:

- The longitudinal vehicle velocity, derived from wheel speed measurements, is assumed to be under limited slip conditions. Although this may not hold under some extreme scenarios, such as racing applications, it is generally not a concern as we combine data points from the four corners . In practice, as evidenced in the validation results in Section 3, this assumption does not pose significant issues. For additional precision, alternative approaches like sensor fusion between the Inertial Measurement Unit (IMU) and GPS can be employed to ascertain longitudinal vehicle velocities [18].
- Steering angle measurements, obtained from a steering-mounted encoder, are combined with a kinematic map of the steering system to calculate the left and right wheel angles (respectively δ_l and δ_r). In the context of the bicycle model, the steering angle for the dynamic model is obtained as the average angle of both front wheels:

$$\delta = \frac{\delta_l + \delta_r}{2}. \tag{5}$$

It is worth emphasizing that to avoid substantial bias on the identified quantities, these input measurements should be relatively noise-free. Therefore, employing low-pass filtering may be necessary in practice to ensure accurate results. Furthermore, to ensure the typical condition of persistent excitation [3], datasets with sufficient variations in these inputs should be considered. Assuming sufficiently long driving horizons, this condition should not pose any significant issues.

In most, if not all, modern automotive systems, two sensors that provide vital information on lateral vehicle behavior—predominantly dependent on the front and rear cornering stiffnesses—are present:

- Lateral acceleration a_y: This sensor measures the vehicle's absolute acceleration in the lateral direction, and can be modelled as follows:

$$a_y = -\frac{1}{mv_x}(c_f + c_r)v_y + \frac{1}{mv_x}(-l_f c_f + l_r c_r)\omega_z + \frac{1}{m}c_f\delta. \tag{6}$$

  Please note that the coupling term between v_x and ω_z is absent compared to Eq. (1a), as the accelerometer measures the absolute lateral acceleration instead of the local sideslip velocity variation. Using these equations directly for identification purposes is challenging at low velocities when $v_x \approx 0$ due to ill-conditioning of the problem (as the linear tire model is no longer valid in such cases). Since we do not explicitly need to solve or integrate these equations for force evaluation or time evolution, we can effectively address this issue by multiplying the full equation by v_x:

$$mv_x a_y = -(c_f + c_r)v_y + (-l_f c_f + l_r c_r)\omega_z + c_f v_x \delta. \tag{7}$$

  If the perfect parameters and lateral velocity (or a sufficiently close approximation) could be identified, this would mean that the following goal function should

be near zero:

$$g_{a_y} = -mv_x a_y - (c_f + c_r)v_y + (-l_f c_f + l_r c_r)\omega_z + c_f v_x \delta \approx 0. \tag{8}$$

- Yaw rate ω_z: The second dynamic sensor measurement we can utilize is the yaw rate. However, to connect this to vehicle dynamics, we also need to calculate the yaw acceleration. In this work, we propose using central differencing to derive the yaw acceleration from measured rates:

$$\dot{\omega}_z(t_i) \approx \frac{\omega_z(t_{i+1}) - \omega_z(t_{i-1})}{2\Delta t}. \tag{9}$$

Low-pass filtering of the yaw rate measurement and the derived acceleration might be required to manage noise levels. This is not a major concern, as typical sampling rates in automotive systems are around 100Hz, significantly faster than common lateral dynamics responses. Using the yaw rate measurement and derived acceleration, the following equation can be evaluated:

$$\dot{\omega}_z = \frac{1}{I_z v_x}(-l_f c_f + l_r c_r)v_y - \frac{1}{I_z v_x}(l_f^2 c_f + l_r^2 c_r)\omega_z + \frac{1}{I_z} l_f c_f \delta. \tag{10}$$

Similar to the earlier case, using these equations directly is problematic at very low velocities when $v_x \approx 0$. We address this by multiplying the full equation by v_x:

$$I_z v_x \dot{\omega}_z = (-l_f c_f + l_r c_r)v_y - (l_f^2 c_f + l_r^2 c_r)\omega_z + v_x l_f c_f \delta. \tag{11}$$

This leads to the following objective function for the dynamic model:

$$g_{\omega_z} = -I_z \omega_z \dot{\omega}_z + (-l_f c_f + l_r c_r)v_y - (l_f^2 c_f + l_r^2 c_r)\omega_z + v_x l_f c_f \delta \approx 0. \tag{12}$$

Every sampling instance of the vehicle sensor system, for example, a Controller Area Network (CAN) bus, permits us to evaluate these equations. In automotive applications, this information is typically available at a frequency of approximately 100Hz.

In certain instances, supplementary data might be accessible, which could be employed to deliver additional regularization. For example, the kinematic relationship for the derivative of the local lateral velocity could be exploited:

$$\dot{v}_y = a_y - \omega_z v_x. \tag{13}$$

Nonetheless, according to the authors' experience, this does not significantly impact the identification results. In high-end testing scenarios, if optical lateral velocity measurements (albeit noisy) are available, these could be added as additional regularization functions. However, in the present study, we limit the assumptions to the two aforementioned objective functions.

Taking into account the previously mentioned known parameters, inputs, and measurement functions, we are left with the following variables to be identified:

- The front and rear cornering stiffnesses, c_f and c_r, which are assumed to be constant over all the n time steps considered.

- The lateral vehicle velocity, $v_{y,i}$, which needs to be identified for all n time steps i.

For all n time steps, we can then formulate the two objective functions in terms of these unknown variables as:

$$\mathbf{g}_{a_y}(c_f, c_r, \mathbf{v}_y) = \begin{bmatrix} g_{a_y}(t_1, c_f, c_r, v_{y,1}) \\ \vdots \\ g_{a_y}(t_n, c_f, c_r, v_{y,n}) \end{bmatrix}, \tag{14}$$

$$\mathbf{g}_{\omega_z}(c_f, c_r, \mathbf{v}_y) = \begin{bmatrix} g_{\omega_z}(t_1, c_f, c_r, v_{y,1}) \\ \vdots \\ g_{\omega_z}(t_n, c_f, c_r, v_{y,n}) \end{bmatrix}, \tag{15}$$

The number of equations in this case is $2n$, and the number of unknowns is $n+2$. This indicates that, in theory, the system might be identifiable if we have at least two time steps. However, in practice, there are additional considerations to account for. Firstly, the robustness to model and measurement noise is critical. This factor encourages the use of a larger number of time steps to improve the reliability of the identification. Moreover, the different time steps should represent different driving conditions. In other words, multiple samples from a straight driving scenario will not lead to an identifiable problem, and neither will measurements from a single steady-state corner. Fortunately, these edge cases do not represent realistic driving scenarios, so identifiability is not typically an issue in practice. It's crucial to select time steps that represent varied driving conditions to ensure the effectiveness of the identification process. The unique aspects of the proposed scheme when compared to existing estimation methods merit emphasis. Previous works utilizing estimators to track tire parameters necessitate certain treatments to guarantee stability during steady-state instances [9,17]. Unlike these methodologies, the proposed approach bypasses the requirement for such specialized handling. Estimation-based strategies, as a rule, demand continuous excitation of lateral dynamics across each and every time step. The proposed method diverges significantly from this prerequisite. It merely requires a sufficient number of instances with excitation over the fully considered time window, offering more flexibility and making it less demanding in terms of the quality of the dataset. Additionally, an advantage of the proposed methodology is that it does not mandate consecutive time steps, presenting the opportunity to exclude certain time steps that do not contribute significantly to the identification process. This presents an additional degree of robustness to the system identification approach. In this study, we operate under the assumption that all time steps within a selected time window are taken into account. However, it opens an interesting avenue for future research. Investigations can be focused on the potential benefits and efficiency gains by carefully selecting time steps, which could lead to further refinements in the identification process. Such refinements could potentially improve both the efficiency and precision of the identification scheme across a wider range of operating conditions.

One crucial aspect to consider in the construction and evaluation of these measurement goal functions is the noise inherently present in the available measurements (i.e., vehicle velocity, steering angle, lateral acceleration, and yaw rate). While least-squares identification is generally robust against output noise, input noise can significantly bias the results [7,15]. Therefore, it is essential to apply appropriate filters to the available measurements, aiming to mitigate bias errors in the identified parameters. A significant

advantage of the proposed framework is its ability to process measurements in batches, which enables the use of non-causal filters. Non-causal filters can often offer practical benefits over their causal counterparts, leading to improved overall results within the identification framework [12]. In this study, we employ a moving average filter as implemented in Matlab's *smoothdata*-function [10]. The mathematical formulation of this filter is as follows:

$$y(t_i) = \frac{1}{n_- + n_+ + 1} \sum_{j=-n_-}^{n_+} x(t_{i+j}), \tag{16}$$

where n_- and n_+ respectively represent the number of elements considered before and after the current element in the noisy signal x. The result is a filtered signal y, where the noise has been effectively minimized. Depending on the available sensors and sampling rates, some tuning of these smoothing lengths will be necessary.

2.3. Weighted least-squares optimization framework

The two types of measurement goal functions described previously can be transformed into least-square objective functions:

$$|\mathbf{g}_{a_y}|_2^2 = \frac{1}{2}\mathbf{g}_{a_y}^T \mathbf{g}_{a_y}, \quad |\mathbf{g}_{\omega_z}|_2^2 = \frac{1}{2}\mathbf{g}_{\omega_z}^T \mathbf{g}_{\omega_z}. \tag{17}$$

These two least-squares functions can be combined in a weighted fashion into a single objective function $\mathcal{G}$:

$$\mathcal{G}(\mathbf{v}_y, c_f, c_r) = w_{a_y}|\mathbf{g}_{a_y}|_2^2 + w_{\omega_z}|\mathbf{g}_{\omega_z}|_2^2. \tag{18}$$

In the above equations, w_{a_y} and w_{ω_z} represent weights assigned to the least-squares functions associated with lateral acceleration and yaw rate, respectively. These weights allow for customization and tuning of the objective function based on the specific application or the precision of the involved sensors. For the validation in Sec. 3 we will evaluate the impact of these weights. From these validations we have observed that a relatively higher w_{ω_z} consistently leads to better identification results.

This weighted objective function forms the core of the nonlinear optimization problem which we can solve to identify the tire stiffness parameters and the corresponding lateral velocities. This can be expressed as:

$$\min_{\mathbf{v}_y, c_f, c_r} \mathcal{G}(\mathbf{v}_y, c_f, c_r), \tag{19}$$

where $\mathbf{v}_y \in \mathbb{R}^n$ is a vector containing the identified lateral velocities at the considered n time steps. Although this constitutes a nonlinear optimization problem, the nonlinearity is relatively moderate and the (approximate) Jacobians required to solve the problem can be evaluated with high efficiency, as discussed in the forthcoming section. As we will see in Sec. 3, this enables a highly efficient identification scheme that can operate several orders of magnitude faster than real-time.

2.4. Solution algorithm

In this work we employ a gradient based optimization scheme to solve the evisaged least-squares problem [19]. When solving these least-squares problems, these algorithms typically require the Jacobians of the measurement goals to compute respective gradients. In this case, the objective function $\mathcal{G}(\mathbf{v}_y, c_f, c_r)$ is a function of the lateral velocities $\mathbf{v}_y$ at each time step and the front and rear cornering stiffnesses c_f and c_r and the corresponding derivatives can be written as:

$$\frac{\partial \mathcal{G}}{\partial \mathbf{v}_y} = w_{a_y} \frac{\partial \mathbf{g}_{a_y}}{\partial \mathbf{v}_y}^T \mathbf{g}_{a_y} + w_{\omega_z} \frac{\partial \mathbf{g}_{\omega_z}}{\partial \mathbf{v}_y}^T \mathbf{g}_{\omega_z} \tag{20}$$

$$\frac{\partial \mathcal{G}}{\partial c_f} = w_{a_y} \frac{\partial \mathbf{g}_{a_y}}{\partial c_f}^T \mathbf{g}_{a_y} + w_{\omega_z} \frac{\partial \mathbf{g}_{\omega_z}}{\partial c_f}^T \mathbf{g}_{\omega_z} \tag{21}$$

$$\frac{\partial \mathcal{G}}{\partial c_r} = w_{a_y} \frac{\partial \mathbf{g}_{a_y}}{\partial c_r}^T \mathbf{g}_{a_y} + w_{\omega_z} \frac{\partial \mathbf{g}_{\omega_z}}{\partial c_r}^T \mathbf{g}_{\omega_z}. \tag{22}$$

The Jacobian matrix for this system, would be of size $(2n) \times (n+2)$ where n is the number of timesteps. The entries of this matrix represent how small changes in the lateral velocities and cornering stiffnesses would affect the lateral acceleration and yaw rate. Starting from Eq. (8) we can evaluate these derivatives for $\mathbf{g}_{a_y}$ in more detail:

$$\frac{\partial \mathbf{g}_{a_y}}{\partial \mathbf{v}_y} = -(c_f + c_r)\mathbf{I}_n, \tag{23}$$

$$\frac{\partial \mathbf{g}_{a_y}}{\partial c_f} = \left[-\mathbf{v}_y - l_f \boldsymbol{\omega}_z + \mathbf{v}_x \boldsymbol{\delta}\right], \tag{24}$$

$$\frac{\partial \mathbf{g}_{a_y}}{\partial c_r} = \left[-\mathbf{v}_y + l_r \boldsymbol{\omega}_z\right], \tag{25}$$

where $\mathbf{I}_n$ represents a $n \times n$ unity matrix. Similarly from Eq. (12) we get the derivatives for $\mathbf{g}_{\omega_z}$:

$$\frac{\partial \mathbf{g}_{\omega_z}}{\partial \mathbf{v}_y} = (-l_f c_f + l_r c_r)\mathbf{I}_n, \tag{26}$$

$$\frac{\partial \mathbf{g}_{\omega_z}}{\partial c_f} = \left[-l_f \mathbf{v}_y - l_f^2 \boldsymbol{\omega}_z + l_f \mathbf{v}_x \boldsymbol{\delta}\right], \tag{27}$$

$$\frac{\partial \mathbf{g}_{\omega_z}}{\partial c_r} = \left[l_r \mathbf{v}_y - l_r^2 \boldsymbol{\omega}_z\right]. \tag{28}$$

The problem at hand exhibits a highly structured and sparse nature, allowing for efficient resolution using standard optimization tools. Indeed, the complexity and sparsity of the problem lend themselves to rapid computation, capable of processing extensive data ranging from several minutes to hours within just a few seconds. This ensures that even large-scale data can be tackled without imposing significant computational burden. In this study, we have employed the *lsqnonlin* function available in Matlab to solve the envisaged least-squares problem with the default *trust-region-reflective* algorithm [10]. However, it should be noted that this approach is not exclusively tied to this particular tool. A wide array of generally available least-squares optimizers can be utilized for this purpose, thereby enhancing the accessibility and flexibility of the so-

lution method. Further demonstration of the computational efficiency and robustness of the proposed methodology will be provided in the forthcoming validation section.

3. Validation

This section details the validation of the proposed identification scheme. To ensure the clarity and transparency of our study, we utilize two open-source validation platforms, which are discussed in Sec. 3.1. Subsequent sections present the identification results for each case, providing a comprehensive analysis that includes a discussion on tuning influence and computational load associated with the identification process..

3.1. Validation platforms

In this work, two validation platforms are employed for which data is available in literature. The considere platforms are shown in Fig. 2.

(a) Ferrari 250LM [11] (b) Range Rover Evoque [17]

Figure 2. Test vehicles for validation.

- Ferrari 250LM: The first vehicle concerns a historic Ferrari 250LM for which a set of measurements is performed in racing conditions [14]. This platform is equipped with a high end IMU which can also provide reference data for the lateral velocity. Various test data is available online [13]. For this platform, the longitudinal vehicle velocity is evaluated at the centre of gravity and available from the IMU system. For this analysis, the data is used from the first session and first outing on Februari 21st 2014. The results are discussed in Sec. 3.2.
- Range Rover Evoque: The test vehicle is an electrified Range Rover Evoque provided by Flanders Make. For the tests, the vehicle is equipped with several sensors: a low-cost Global Navigation Satellite System (GNSS) receiver, an inertial measurement unit (IMU) and a Corrsys Datron optical sensor which provide reference data on the lateral velocity [17]. In this case, the longitudinal vehicle velocity is obtained by averaging the four wheel speeds. Several test data is openly availabe for this vehicle [26]. For this work we have used the dataset for medium speed at a durability test track. The results are discussed in Sec. 3.3.

In both cases, the bicycle model steering angle δ is taken as the average of the left and right front wheel angles:

$$\delta = \frac{\delta_{fl} + \delta_{fr}}{2}. \tag{29}$$

In both cases the lateral acceleration and yaw rate measurements are available from an IMU system. It is to be noted that these are not common production IMU systems, and their accuracy is expected to be superior to what is available at the CAN bus of a regular production vehicle.

The vehicle parameters necessary for evaluating the bicycle models as employed in this work, are presented in table 1. An important point to notice, is that both

Table 1. Vehicle bicycle model parameters

		250LM	Evoque	Units
m	Vehicle mass	982	2442	kg
I_{zz}	Yaw moment of inertia	1365	3231	kgm^2
l_f	Distance between COG and front axle	1.33	1.44	m
l_r	Distance between COG and rear axle	1.07	1.24	m

testing platform have a center-of-gravity which is closer to the rear than the front axle, which is unlike most commonly available vehicles and might provide some additional challenges in terms of maintaining stable analyses. However, this should not influence the generalizability of the conclusions in this validation. Notice that overall these vehicles are from a different era, consist of a very different topology and are in a different weight class, which is ideal for validating the general applicability of the presented framework.

In order to validate the identified parameters, we employ the dynamic bicycle model delineated in Sec. 2.1 and Eq. (4). With the measured steering angle δ and longitudinal vehicle velocity v_x serving as inputs, we use the identified front and rear cornering stiffnesses as parameters (in conjunction with the quantities itemized in Tab. 1) to perform a forward dynamic simulation. The simulated lateral acceleration a_y^{sim}, yaw rate ω_z^{sim}, and sideslip velocity v_y^{sim} are compared to their respective measured values ($.^{rev}$) to assess the precision of the identified parameters. It is essential to note here that the proposed identification algorithm does not employ a forward simulation during the identification process. This makes the evaluation procedure inherently resistant to overfitting the specific case.

3.2. Ferrari 250LM results

To validate our approach using the Ferrari case study, we chose a time window of $250s$, sampling data at a frequency of $100Hz$. This results in a total of $n = 25000$ time instances under consideration. All data is processed using the moving average filter (Eq. (16)) with $n_- = n_+ = 10$. For this specific case, Fig. 3 depicts the filtered steering angle and longitudinal velocity. This case illustrates a dynamic driving cycle, encompassing high velocities and substantial steering inputs. Noteworthy is the presence of realistic imperfections in the data, such as a sudden corrective steering input around $t = 70s$. Additionally, longer straight driving sections are also included ($t = 80-110s$), which could potentially pose challenges for estimation-based approaches due to the absence of excitation. Consequently, this case serves as a demanding and practical dataset for the identification of vehicle dynamics.

As previously discussed in Sec. 2.3, the balance between the two types of measurement goals can significantly impact the results of the identification process. To examine these influences, we maintain a fixed value of $w_{a_y} = 1$ while varying w_{ω_z} among the

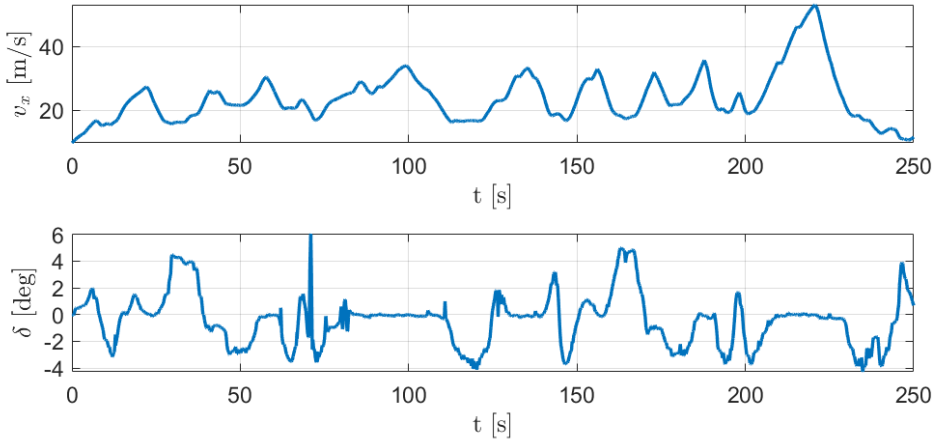

Figure 3. Ferrari LM 250 input measurements

values 1, 10, 100, and 1000. The resulting front and rear cornering stiffnesses for these variations are depicted in Fig. 4. In addition to these results, the figure also provides

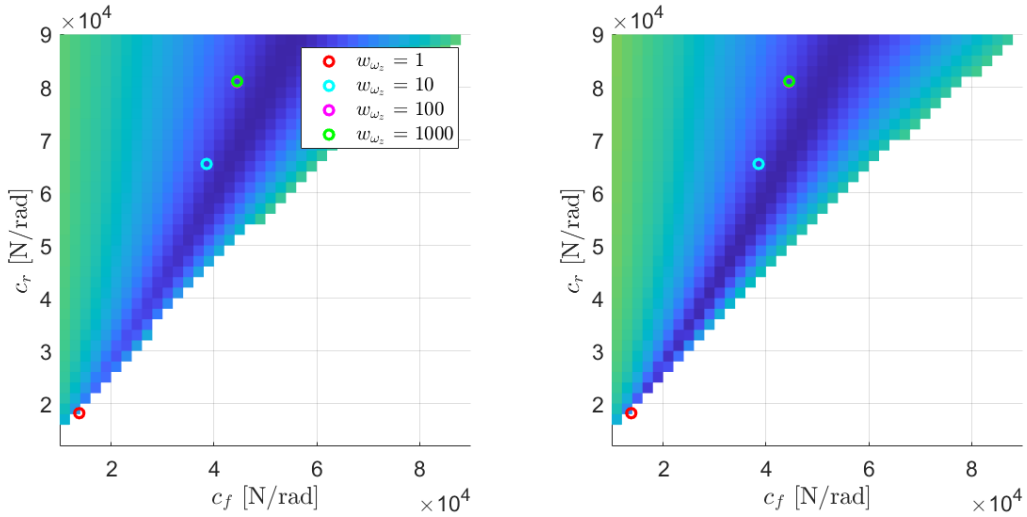

(a) $|a_y^{ref} - a_y^{sim}|_2^2$ (b) $|\omega_z^{ref} - \omega_z^{sim}|_2^2$

Figure 4. Ferrari 250LM identified cornering stiffnesses and error on simulated response as a function of the cornering stiffness

the simulation error associated with varying cornering stiffnesses, offering insight into the efficacy of the proposed scheme compared to the result that could be obtained from a simulation based optimization. It should be noted that no results are presented for cases where c_f is significantly higher than c_r due to resultant model instability. Upon analyzing the errors as a function of cornering stiffnesses, it is apparent that there is a high sensitivity in obtaining the correct ratio of front and rear cornering stiffnesses, whereas their absolute values have a lesser impact on the final error. The figure illustrates that a relatively low w_{ω_z} leads to an underestimation of cornering stiffnesses. As the relative weight increases, the identified cornering stiffnesses increase, seeming to plateau when $w_{\omega_z} = 100$. At $w_{\omega_z} = 1000$, the identified parameters remain virtually

unchanged, indicating that the process has reached a saturation point.

To further understand the impact on the dynamics, we examine the progression of the simulated and measured response for the identified parameters of the four cases, alongside the measured reference, as displayed in Fig. 5. These results provide some

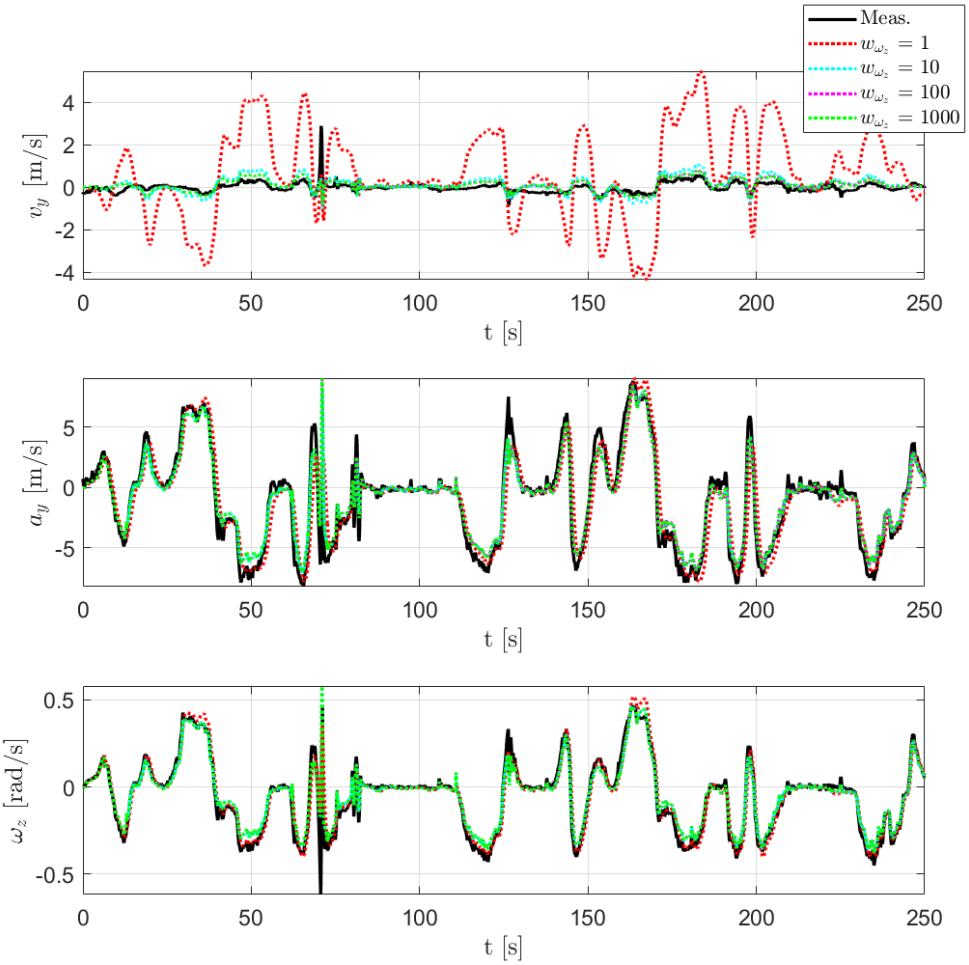

Figure 5. Ferrari 250LM measured and simulated response

intriguing insights. When considering the measured a_y and ω_z, the simulations with the identified parameters all provide rather good accuracy. The most accurate of the two measured quantities transitions from the lateral acceleration to the yaw rate as the weights change, which aligns with the findings presented in Fig. 4. In addition, we compare the simulated and measured lateral velocity, v_y. It becomes clear that the higher cornering stiffnesses resulting from the larger w_{ω_z} values lead to significantly more accurate lateral velocity values. These outcomes appear very reliable in absolute terms, even though the lateral velocity behavior was not directly considered in the identification process. This result is particularly promising if the identified model is to be utilized for purposes such as lateral control.

Lastly, it is pertinent to evaluate the convergence behavior and computational load of the proposed approach, as illustrated in Fig. 6. As one might expect, enhancing the

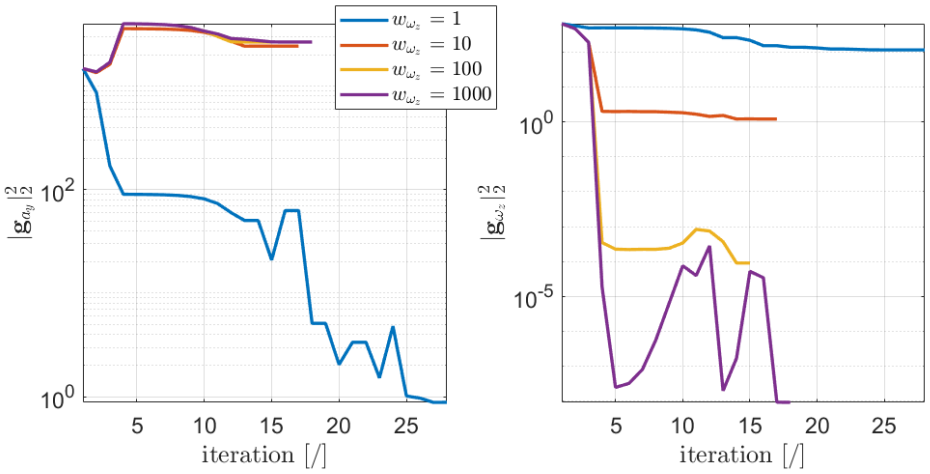

Figure 6. Ferrari 250LM nonlinear least-squares convergence

weight on the yaw rate measurement goal w_{ω_z} results in a higher minimum value for the lateral acceleration measurement goal, but a lower value for the yaw rate measurement goal. The four cases illustrate rapid convergence to a final value, indicating the minimal impact of the nonlinearity of the optimization problem under consideration. In this instance, we apply the standard stopping criterion of the Matlab *lsqnonlin*-function, but the results suggest that five to ten iterations are adequate to achieve a satisfactory outcome. For the final three cases, requiring approximately 17 iterations, the optimization takes less than one second to execute the identification on this $250s$ measurement set on a standard laptop (Intel(R) Core(TM) i7-12800H, 2.4GHz). This finding suggests that the approach presented herein could be effectively used to process real-time driving data at a faster-than-real-time rate if, for instance, the maximum number of iterations is fixed.

3.3. Range Rover Evoque results

For enhanced validation and consistency of the results, we carry out a similar analysis for the Range Rover Evoque dataset. The evolution of the considered longitudinal velocity and steering input is depicted in Fig. 7. This dataset encompasses over $313s$ of recorded data, available at a sampling frequency of $500Hz$ (although it should be highlighted that some of this data has been resampled from the original data at 100Hz), resulting in a total of $n = 160000$ time steps under consideration. All data is subjected to the moving average filter (Eq. (16)) with $n_- = n_+ = 10$, but for the (numerically derived) yaw acceleration, we employed $n_- = n_+ = 50$ to achieve a sufficiently smooth behavior.

Firstly, we assess the variation in the identified cornering stiffness as we adjust the weights, as depicted in Fig. 8. We observe a similar behavior to the previous case, where increasing w_{ω_z} results in higher stiffnesses and convergence seems to occur around $w_{\omega_z} = 100$. We also observe a consistent trend where the proposed approach leads to a slight overestimation of the rear cornering stiffness compared to the front cornering stiffness, where the model error reaches its minimum.

When we compare the simulated responses, based on these identified parameters, with the available measurements as depicted in Fig. 9, a similar pattern to the previ-

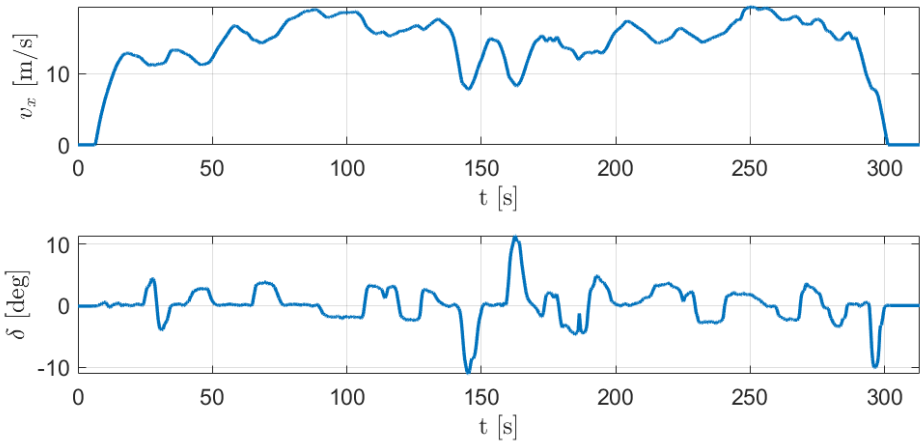

Figure 7. Range Rover Evoque input measurements

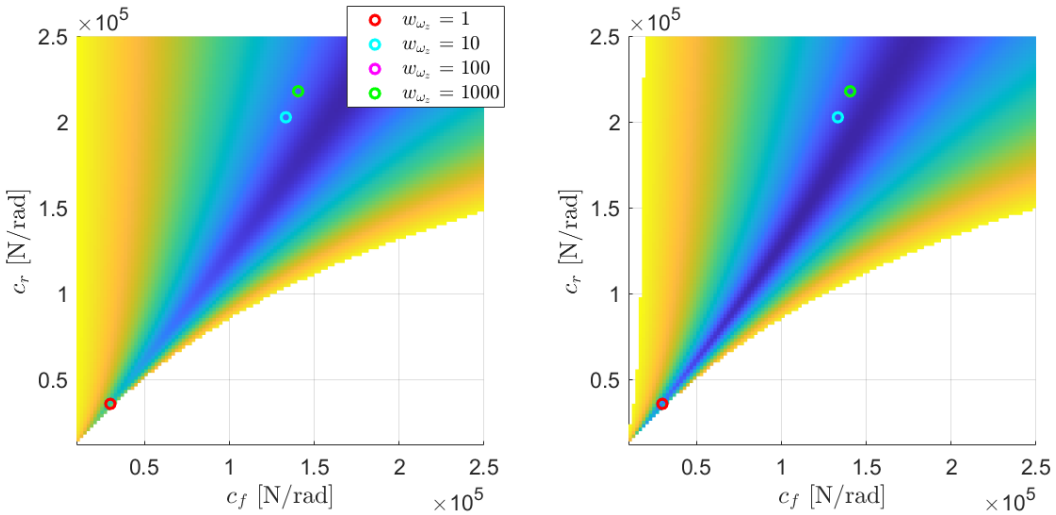

(a) $|a_y^{ref} - a_y^{sim}|_2^2$ (b) $|\omega_z^{ref} - \omega_z^{sim}|_2^2$

Figure 8. Range Rover Evoque error on simulated response

ous case is discernible. Across all test scenarios, the two reference measurements are

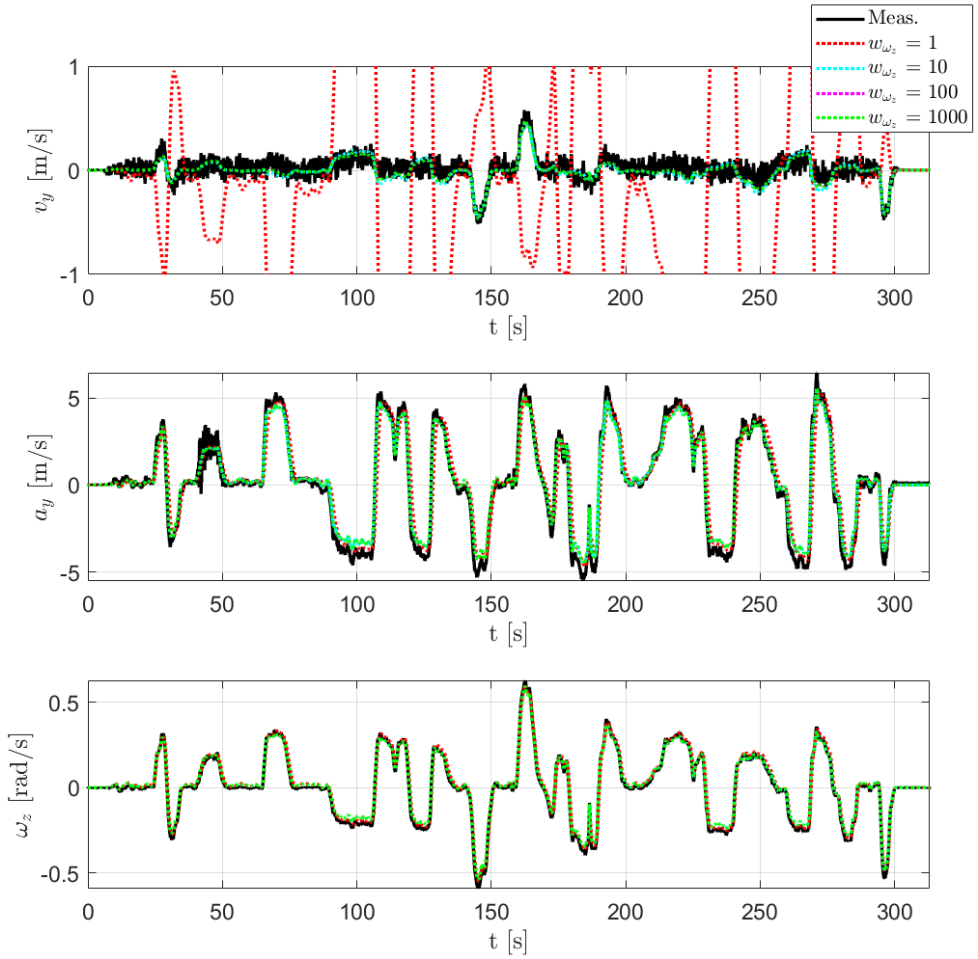

Figure 9. Range Rover Evoque measured and simulated response

accurately mirrored in the simulations, but it's notable once again that the lateral velocity is precisely approximated only by the models identified with higher cornering stiffnesses when w_{ω_z} is raised. This finding is quite remarkable as it implies the same tuning of the identification algorithm yields entirely analogous results, even when applied to dramatically different types of vehicles.

Finally, we examine the convergence behavior for this case, as illustrated in Fig. 10. Similar to the previous case, adjusting the weights determines the extent of minimization for each function. Interestingly, for this case, we encounter more complex convergence when $w_{\omega_z} = 1000$. This could potentially be due to the greater noise in the yaw rate measurements (and their numerical derivatives) in comparison to the prior scenario. Consequently, it is advisable to avoid overly amplifying w_{ω_z} and instead to opt for a moderate value.

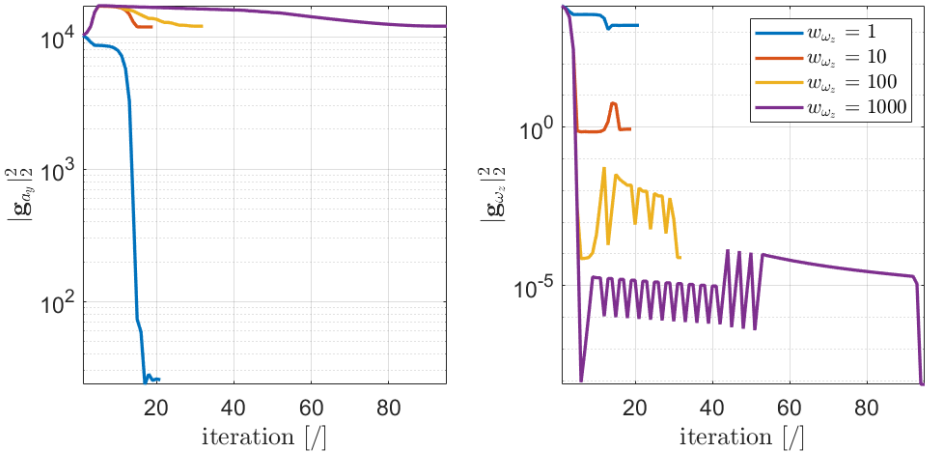

Figure 10. Range Rover Evoque nonlinear least-squares convergence

4. Conclusion

This work introduces and validates an approach that exploits nonlinear least-squares techniques for cornering stiffness estimation. The methodology was effectively tested on two distinct vehicle datasets – the Ferrari LM 250 and the Range Rover Evoque, with results offering crucial insights into the identification process, particularly with respect to the weighting of measurement goals and the associated impacts. Furthermore, an intriguing outcome from the research was the identification of similar patterns in the results obtained from two drastically different vehicle types, a testament to the robustness of the identification algorithm. The convergence behaviour of the nonlinear least-squares approach was also explored, providing critical information for the optimization of future algorithm tuning. Looking forward, there are several promising avenues for further research. One such direction could involve exploring the integration of this approach with piecewise linear tire models to more effectively capture e.g. saturation phenomena. This could lead to a more nuanced understanding of vehicle behavior under different driving conditions. Another potentially rewarding line of inquiry could be the validation of this approach on open road data. The two datasets used in this study were track data, which do not fully represent the dynamics of regular driving. By applying the algorithm to open road data, we could further validate its effectiveness and versatility, which would significantly enhance its practical value.

Acknowledgment

The KU Leuven Research Fund is gratefully acknowledged for its support. Flanders Make. The Flanders Innovation & Entrepreneurship Agency within the AI4Test project is gratefully acknowledged for its support. This research was partially supported by Flanders Make, the strategic research centre for the manufacturing industry.

References

[1] Kistler, measuring systems and sensors. www.kistler.com.

[2] *Bosch Automotive Handbook*. Robert Bosch, 9 edition, 2014.
[3] B. Armstrong. On finding'exciting'trajectories for identification experiments involving systems with non-linear dynamics. In *Proceedings. 1987 IEEE International Conference on Robotics and Automation*, volume 4, pages 1131–1139. IEEE, 1987.
[4] T. Ba, X. Guan, J. W. Zhang, and S. Wang. Application of recursive subspace method in vehicle lateral dynamics model identification. *Mathematical Problems in Engineering*, 2016, 2016.
[5] G. Baffet, A. Charara, and J. Stéphant. Sideslip angle, lateral tire force and road friction estimation in simulations and experiments. *Computer Aided Control System Design, 2006 IEEE International Conference on Control Applications, 2006 IEEE International Symposium on Intelligent Control, 2006 IEEE*, pages 903–908, 2006.
[6] D. Chindamo, B. Lenzo, and M. Gadola. On the vehicle sideslip angle estimation: a literature review of methods, models, and innovations. *applied sciences*, 8(3):355, 2018.
[7] G. H. Golub and C. F. Van Loan. An analysis of the total least squares problem. *SIAM journal on numerical analysis*, 17(6):883–893, 1980.
[8] M. Grewal and K. Glover. Identifiability of linear and nonlinear dynamical systems. *IEEE Transactions on automatic control*, 21(6):833–837, 1976.
[9] C. T. Hsu, L. Vehicle dynamic prediction systems with on-line identification of vehicle parameters and road conditions. *Sensors*, 12:15778–15800, 2012.
[10] M. Inc. Matlab – the language of technical computing, lsqnonlin function. Software available at https://www.mathworks.com/help/optim/ug/lsqnonlin.html, 2021. Accessed: 2022-06-14.
[11] R. Institute, 2023. https://revsinstitute.org/the-collection/1965-ferrari-250-lm/.
[12] J. R. Jensen, J. Benesty, M. G. Christensen, and S. H. Jensen. Non-causal time-domain filters for single-channel noise reduction. *IEEE transactions on audio, speech, and language processing*, 20(5):1526–1541, 2012.
[13] J. C. Kegelman, L. K. Harbott, and J. C. Gerdes, 2016. 2014 Targa Sixty-Six. Stanford Digital Repository. Available at: http://purl.stanford.edu/hd122pw0365.
[14] J. C. Kegelman, L. K. Harbott, and J. C. Gerdes. Insights into vehicle trajectories at the handling limits: analysing open data from race car drivers. *Vehicle system dynamics*, 55(2):191–207, 2017.
[15] I. Markovsky and S. Van Huffel. Overview of total least-squares methods. *Signal processing*, 87(10):2283–2302, 2007.
[16] F. Naets. State and parameter estimation for vehicle dynamics. In *Vehicle Dynamics: Fundamentals and Ultimate Trends*, pages 235–288. Springer, 2021.
[17] F. Naets, S. van Aalst, B. Boulkroune, N. El Ghouti, and W. Desmet. Design and experimental validation of a stable two-stage estimator for automotive sideslip angle and tire parameters. *IEEE Transactions on Vehicular Technology*, 66(11):9727–9742, 2017.
[18] X. Niu, S. Nassar, and N. EL-SHEIMY. An accurate land-vehicle mems imu/gps navigation system using 3d auxiliary velocity updates. *Navigation*, 54(3):177–188, 2007.
[19] J. Nocedal and S. J. Wright. *Numerical optimization*. Springer, 1999.
[20] H. B. Pacejka. *Tire and Vehicle Dynamics*. SAE, Inc., 2 edition, 2006.
[21] L. Ray. Nonlinear state and tire force estimation for advanced vehicle control. *IEEE Transactions on Control Systems Technology*, 3(1):117–124, 1995.
[22] L. Ray. Nonlinear tire force estimation and road friction identification: simulation and experiments. *Automatica*, 33(10):1819–1833, 1997.
[23] J. Ryu. *State and parameter estimation for vehicle dynamics control using GPS*. PhD thesis, Standford University, December 2004.
[24] M. Segel. Theoretical prediction and experimental substantiation of the response of the automobile to steering control. In *Proceedings of the Institution of Mechanical Engineers: Automobile Division*, volume 10, pages 310–330, January 1956.
[25] Tass. Tyre testing. https://www.tassinternational.com/tyre-testing.
[26] C. Vaseur and S. Van Aalst, 2019. Test Results at Ford Lommel Proving Ground ESR 11 (Final) [Data set], Zenodo, https://doi.org/10.5281/zenodo.3263811.

[27] B. A. H. Vicente, S. S. James, and S. R. Anderson. Linear system identification versus physical modeling of lateral–longitudinal vehicle dynamics. *IEEE Transactions on Control Systems Technology*, 29(3):1380–1387, 2020.

[28] M. Viehweger, C. Vaseur, S. van Aalst, M. Acosta, E. Regolin, A. Alatorre, W. Desmet, F. Naets, V. Ivanov, A. Ferrara, et al. Vehicle state and tyre force estimation: demonstrations and guidelines. *Vehicle system dynamics*, 59(5):675–702, 2021.

[29] P. Yih and J. Gerdes. Steer-by-wire for vehicle state estimation and control. In *Proceedings of the International Symposium on Advanced Vehicle Control (AVEC)*, 2004.